Journal of Alloys and Compounds 509 (2011) 7543–7548

Contents lists available at ScienceDirect

Journal of Alloys and Compounds

journal homepage: www.elsevier.com/locate/jallcom

# Dielectric relaxation, conductivity behaviour and magnetic properties of Mg substituted Ni–Li ferrites

Navneet Singh, Ashish Agarwal, Sujata Sanghi*

*Department of Applied Physics, Guru Jambheshwar University of Science & Technology, Hisar 125001, Haryana, India*

ARTICLE INFO

*Article history:*
Received 31 August 2010
Received in revised form 23 April 2011
Accepted 25 April 2011
Available online 30 April 2011

*Keywords:*
Ferrites
Electrical characterization
Powder diffraction
Dielectric relaxation

ABSTRACT

The dielectric properties of Mg substituted Ni–Li spinel ferrites synthesized by sol–gel auto combustion process have been studied using impedance measurements in the frequency range from 10 Hz to 10 MHz and in the temperature range from 310 K to 473 K. The effect of frequency, temperature and composition on dielectric constant ($\varepsilon'$), dielectric loss ($\tan\delta$) and conductivity ($\sigma$) has been discussed in terms of hopping of charge carriers between $Fe^{2+}$ and $Fe^{3+}$ ions. The electrical modulus formulism has been employed to study the relaxation dynamics of charge carriers and the results indicate the presence of non-Debye type of relaxation in the present ferrites. Similar values of activation energies for dc conduction ($E_{dc}$) and for conductivity relaxation ($E_{M''}$) reveal that the mechanisms of electrical conduction and dielectric polarization are same in these ferrites. A single 'master curve' for normalized plots of all the modulus isotherms observed for a given composition indicates the temperature independence of dynamical process for charge carriers. The saturation magnetization and coercivity have been calculated from the hysteresis loop measurements and show striking dependence on the composition.



## 1. Introduction

Soft ferrites incorporating Li have drawn considerable attention for their potential applications as microwave devices and memory cores. These ferrites possess high resistivity, low dielectric loss, high Curie temperature, saturation magnetization and show interesting hysteresis loop properties [1–4]. These materials have replaced expensive magnetic garnets due to low cost and superior performance [1]. The dielectric and magnetic properties of ferrites can be tailored either by changing the microstructure or by adding different types of metal ions. Ferrites display excellent properties when the microstructure is reduced to nanometer regime [5]. Most commonly used metal ions for improving the properties of ferrites are Ni, Mg, Mn, Zn, Ti, Co etc. Kharabe et al. have studied the dielectric and magnetic properties of Cd substituted Li–Ni ferrites [6]. Soibam et al. have reported the high value of magnetization for Ni–Li–Zn ferrites [7]. The electrical properties of Li–Ni–Eu and Li–Mg–Ti ferrites have been reported by Al-Hilli et al. [8] and by Bellad and Chougule [9], respectively. The properties of ferrites are also dependent on the method of synthesis [10]. The spinel nano-ferrites have been prepared by different techniques such as sol–gel auto combustion, microemulsion and hydrothermal methods [11–13]. The Ni–Li ferrites have been widely used in microwave devices such as circulators, insulators and phase shifters because of their high resistivity, low dielectric loss and excellent magnetic properties. To the best knowledge of investigators, no systematic study of dielectric behaviour in mixed Ni–Li–Mg ferrites has been reported. Therefore, in the present work, influence of $Mg^{2+}$ ions substitution on dielectric and magnetic properties of Ni–Li ferrites prepared by sol–gel auto combustion method have been carried out. Further, an attempt has been made to analyze the dielectric relaxation by modulus formalism to investigate whether Mg substituted Ni–Li ferrites exhibit Debye or non-Debye type of relaxation.

## 2. Experimental

A novel sol–gel auto combustion method was employed to prepare $Ni_{0.5}Li_{1-2x}Mg_xFe_2O_4$ ferrites ($0.0 \le x \le 0.5$). Stoichiometric amount of analytical grade nickel nitrate, lithium nitrate, magnesium nitrate, ferric nitrate and citric acid were dissolved in distilled water. The ratio of metal nitrates to citric acid was 1:1. The pH of the sol was adjusted at 7 by adding ammonia solution to form the gel. The gel was dried at 383 K and then it was ignited to form loose powder. The as prepared powder was annealed at 1073 K to obtain nanosized crystalline powder [14–18]. X-ray diffraction patterns of the annealed ferrites were recorded using Miniflex-II X-ray diffractometer (Rigaku). A Transmission Electron Microscope (Hitachi H-7500) was used to record TEM image of one of the prepared ferrites.

For dielectric measurement, disc shaped pellet having 13 mm diameter was prepared by applying a pressure of 10 tons. The dielectric properties were measured using an impedance/gain phase analyzer (Newtons4th Ltd.) in the frequency range $10^1$–$10^7$ Hz and in the temperature range 310–473 K. The real ($\varepsilon'$) and imaginary ($\varepsilon''$) parts of dielectric constant, loss tangent ($\tan\delta$) and conductivity were calculated using the following relations:

$$\varepsilon' = \frac{Ct}{\varepsilon_0 A} \quad (1)$$

* Corresponding author. Tel.: +91 1662 263384; fax: +91 1662 276240.
*E-mail address:* sutkash@yahoo.com (S. Sanghi).

0925-8388/$ – see front matter © 2011 Elsevier B.V. All rights reserved.
doi:10.1016/j.jallcom.2011.04.126

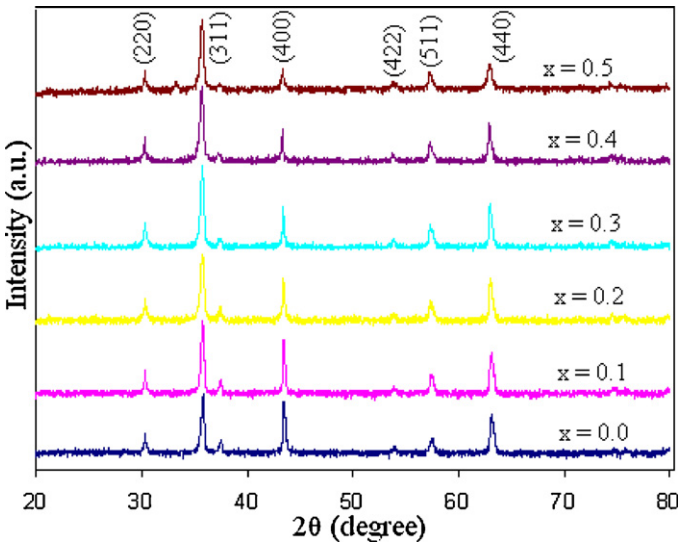


**Fig. 1.** X-ray diffraction patterns of $Ni_{0.5}Li_{1-2x}Mg_xFe_2O_4$ ferrites annealed at 1073 K.

$$\varepsilon'' = \varepsilon' \tan \delta \quad (2)$$

$$\sigma = \varepsilon_o \varepsilon' \omega \tan \delta \quad (3)$$

where $C$ is the capacitance, $t$ is the thickness of the sample, $A$ is the cross-sectional area, $\varepsilon_o$ is the free space permittivity, and $\omega$ is the angular frequency.

Magnetization measurement of the annealed ferrite was carried out using a vibrating sample magnetometer (PAR 155) under applied magnetic field up to 10 kOe at room temperature.

## 3. Results and discussion

### 3.1. XRD analysis

The XRD patterns of the annealed ferrites are shown in Fig. 1. The strong diffraction from the (2 2 0), (3 1 1), (4 0 0), (4 2 2), (5 1 1) and (4 4 0) planes confirm the pure spinel phase of the annealed ferrites [19,20]. The intensities of the (2 2 0), (4 0 0), (4 2 2) and (4 4 0) planes are very sensitive to cation distribution at both the tetrahedral and octahedral sites. The average crystalline size ($D$) of the ferrites is determined from the following Debye–Scherrer formula:

$$D = \frac{K\lambda}{\beta \cos\theta} \quad (4)$$

where $K$ is a constant which depends on the shape of the particle, $\lambda$ is the X-ray wavelength, $\beta$ is the full width at half maximum and $\theta$ is the diffraction angle of the most intense peak, i.e., (3 1 1) [19,21]. The average crystallite size varies from 25 to 29 nm for different concentration of $Mg^{2+}$ ions (Table 1). The lattice constant ($a$) increases with increase in the concentration of $Mg^{2+}$ ions (Table 1). This is obvious because the ionic radius of $Mg^{2+}$ ion is larger than that of $Li^+$ ion. Similar results have been reported for mixed Ni–Li ferrites [6,22].

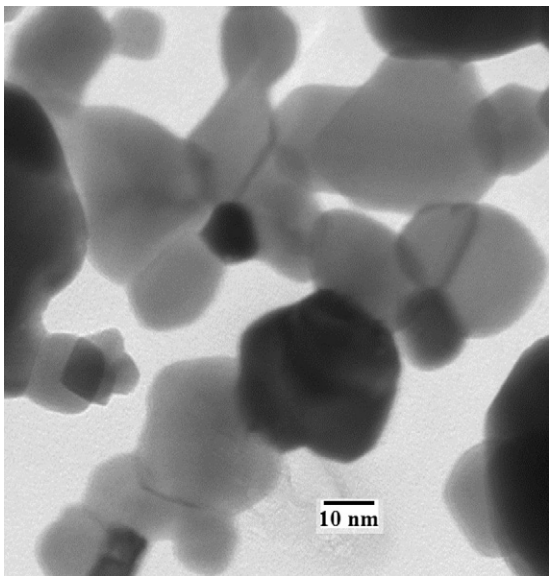


**Fig. 2.** TEM image of $Ni_{0.5}Li_{0.8}Mg_{0.1}Fe_2O_4$ ferrite annealed at 1073 K.

### 3.2. TEM analysis

Fig. 2 shows the TEM image of the $Ni_{0.5}Li_{0.8}Mg_{0.1}Fe_2O_4$ ferrite annealed at 1073 K. The average crystalline size is found to be 30 nm, which agrees well with the XRD results.

### 3.3. Dielectric properties

The dielectric measurements reveal that the dielectric constant ($\varepsilon'$) decreases with increase in frequency as shown in Fig. 3(a) for $x = 0.1$ sample. All other samples show similar frequency dependence of $\varepsilon'$. The variation in $\varepsilon'$ with frequency can be understood on the basis of Maxwell and Wagner two layer model in accordance with Koop's phenomenological theory [23]. The dielectric structure of ferrites is made up of well conducting layer of grains followed by poorly conducting layer of grain boundaries and the high value of dielectric constant arises from the space charge polarization produced at the grain boundary. The polarization mechanism involves the exchange of electrons between the ions of the same element, which are present in more than one valence state and are distributed randomly over crystallographic equivalent sites. Here the exchange of electrons mainly takes place between $Fe^{3+}$ and $Fe^{2+}$ ions present at octahedral sites (B-site). During this exchange mechanism, the electrons have to pass through the grains and grain boundary of the dielectric medium. Owing to high resistance of the grain boundary, the electrons accumulate at the grain boundary and produce space charge polarization. Fig. 3(a) also shows that the dielectric constant decreases rapidly in the low frequency region and becomes frequency independent in the high frequency region.

**Table 1**
Average crystalline size ($D$), Lattice parameter ($a$), dc conductivity ($\sigma_{dc}$), ac conductivity ($\sigma_{ac}$), activation energies for dc conduction ($E_{dc}$) and conductivity relaxation ($E_{M''}$), stretched exponent parameter ($\beta$), saturation magnetization ($M_s$) and coercivity ($H_c$) for $Ni_{0.5}Li_{1.0-2x}Mg_xFe_2O_4$ ferrites.

| $x$ | $D$ (nm) | $a$ (Å) | $\sigma_{dc}$ ($\Omega$ m)$^{-1}$ (at 310 K) | $\sigma_{ac}$ ($\Omega$ m)$^{-1}$ (at 310 K, $10^5$ Hz) | $E_{dc}$ (eV) | $E_{M''}$ (eV) | $\beta$ | $M_s$ (emu/g) | $H_c$ (Oe) |
|---|---|---|---|---|---|---|---|---|---|
| 0.0 | 25 | 8.3346 | $6.76 \times 10^{-7}$ | $1.72 \times 10^{-6}$ | 0.19 | −0.18 | 0.76 | 28.0 | 190 |
| 0.1 | 27 | 8.3346 | $1.57 \times 10^{-6}$ | $2.03 \times 10^{-6}$ | 0.16 | −0.14 | 0.68 | 30.6 | 184 |
| 0.2 | 28 | 8.3379 | $2.77 \times 10^{-6}$ | $6.20 \times 10^{-6}$ | 0.17 | −0.16 | 0.74 | 34.8 | 172 |
| 0.3 | 29 | 8.3413 | $4.19 \times 10^{-6}$ | $6.41 \times 10^{-6}$ | 0.17 | −0.17 | 0.62 | 34.6 | 167 |
| 0.4 | 28 | 8.3446 | $6.94 \times 10^{-6}$ | $1.76 \times 10^{-5}$ | 0.16 | −0.15 | 0.71 | 27.8 | 162 |
| 0.5 | 27 | 8.3479 | $9.41 \times 10^{-6}$ | $1.33 \times 10^{-5}$ | 0.15 | −0.14 | 0.68 | 26.4 | 160 |

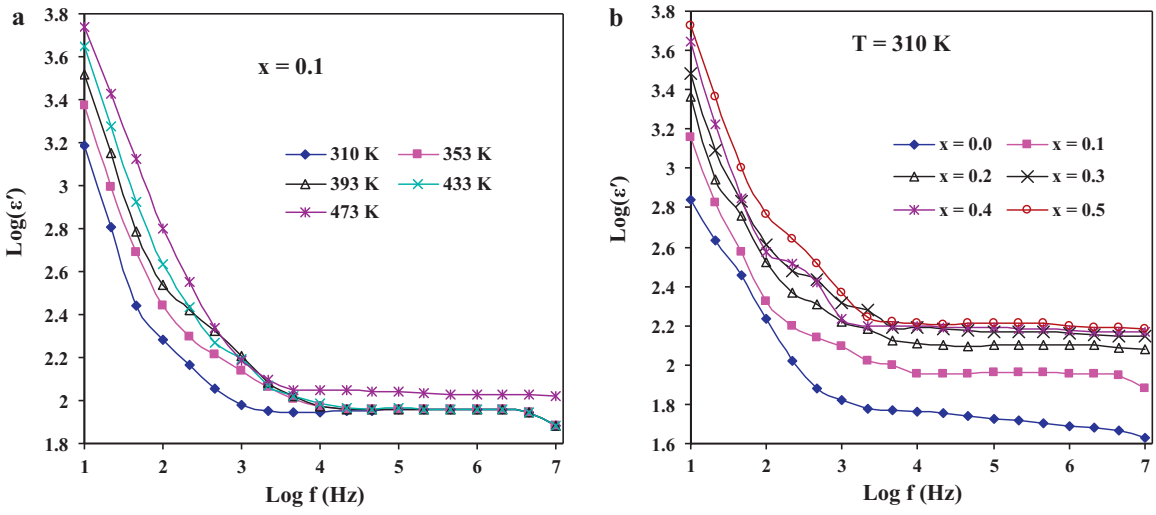


**Fig. 3.** Frequency dependence of real part of dielectric constant ($\varepsilon'$). (a) At various temperatures for $x = 0.1$; (b) at various compositions (at 310 K).

It is well known that the grain boundaries are more effective in low frequency region and the grains are effective in the high frequency region [23]. Therefore, due to the grain boundary effect, the dielectric constant decreases rapidly in the low frequency region. In the high frequency region, the grains come into action and also the hopping of electrons cannot follow the high frequency ac field, therefore, the dielectric constant decreases and becomes frequency independent. It is also observed from Fig. 3(a) that $\varepsilon'$ increases with increase in temperature because the hopping of charge carriers at the octahedral site is thermally activated. Fig. 3(b) shows the frequency dependence of dielectric constant for different values of $x$ at 310 K and it is observed that $\varepsilon'$ increases with increase in the concentration of $Mg^{2+}$ ions. It is known that the $Ni^{2+}$ and $Li^{+}$ ions occupy only the octahedral site (B-site) in the spinel lattice and the $Mg^{2+}$ ions prefer to occupy both the tetrahedral and octahedral sites [24,25]. Therefore, with the increase in the concentration of $Mg^{2+}$ ions, some of the $Mg^{2+}$ ions occupy the tetrahedral site (A-site) and displace the $Fe^{3+}$ ions from A-site to B-site. Thus more $Fe^{2+}$–$Fe^{3+}$ ion pairs are available at B-site for hopping mechanism which results in the increase in dielectric polarization and hence of the dielectric constant. Similar dielectric behaviour has also been observed by Reddy and Rao [26] for Ni–Li ferrites, Shaikh et al. [27] for Li–Mg–Zn ferrites and Ravinder and Reddy [28] for Li–Mg ferrites.

The dielectric loss factor ($\tan\delta$), defined as $\varepsilon''/\varepsilon'$ is a measure of dielectric loss within the ferrite and it arises when the polarization lags behind the applied ac field. The variation of $\tan\delta$ with frequency at different temperatures for $x = 0.1$ sample is shown in Fig. 4(a) and (b) shows the frequency dependence of $\tan\delta$ for different values of $x$ at 310 K. The dielectric loss $\tan\delta$ decreases rapidly in the mid frequency region and in the high frequency region it becomes almost frequency independent (Fig. 4(a)). Such a behaviour can be explained on the basis that in the mid frequency region, which corresponds to low conductivity of grain boundary, more energy is required for electron exchange between $Fe^{2+}$ and $Fe^{3+}$ ions, as a result the loss is higher. In the high frequency region, which corresponds to high conductivity of grain, a small energy is required for electron transfer between the $Fe^{2+}/Fe^{3+}$ ions at the octahedral site. Further, the loss increases with increasing temperature due to the increased conduction of thermally activated electrons (Fig. 4(a)). An important feature (Fig. 4(a)) of this loss factor is the appearance of a peak at all the temperatures and its shifting towards higher frequency with rise in temperature. This peak is observed when the hopping frequency of electrons between $Fe^{3+}$ and $Fe^{2+}$ ions is in resonance with the frequency of applied electric field, i.e., maximum electric energy is transferred to the electrons and the loss shoots up at resonance [19]. The Debye equa-

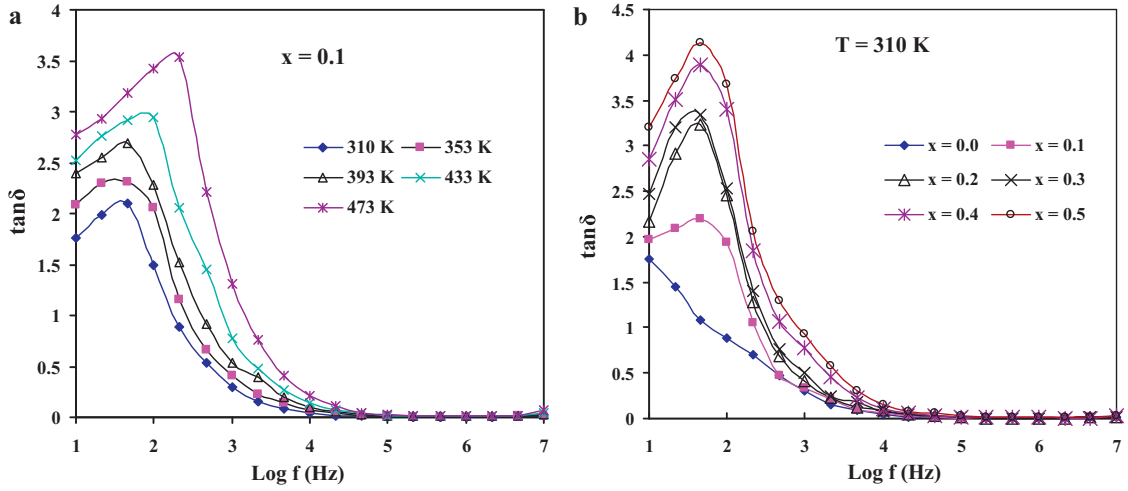


**Fig. 4.** Frequency dependence of loss tangent ($\tan\delta$). (a) At various temperatures for $x = 0.1$; (b) at various compositions (at 310 K).

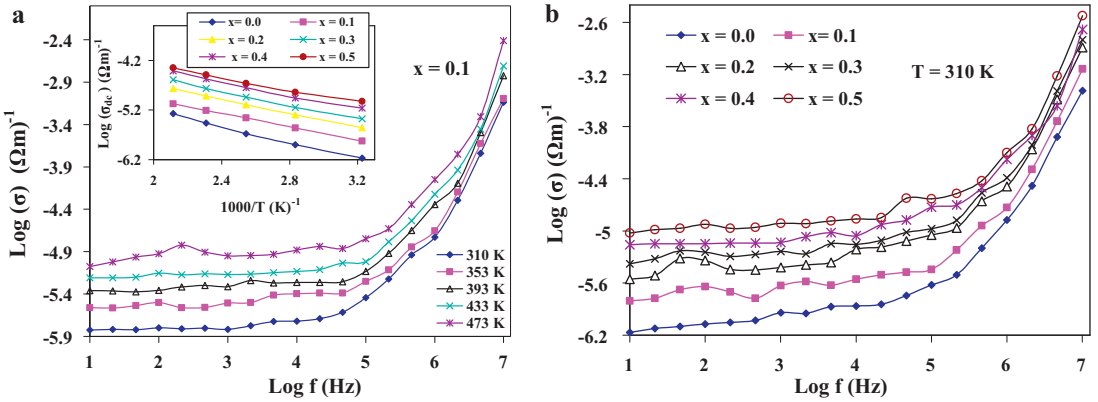


**Fig. 5.** (a) Frequency dependence of conductivity ($\sigma$) for $x = 0.1$ at different temperatures. Inset: Arrhenius plots for the dc conductivity at different compositions. (b) Frequency dependence of conductivity ($\sigma$) for $Ni_{0.5}Li_{1-2x}Mg_xFe_2O_4$ ferrites at 310 K.

tion for the loss tangent is

$$\tan\ \delta = \frac{(\varepsilon_s - \varepsilon_\omega)\omega\tau_{\tan\delta}}{\varepsilon_s + \varepsilon_\omega(\omega\tau_{\tan\delta})^2} \quad (5)$$

where $\varepsilon_s$ and $\varepsilon_\omega$ are the dc and high frequency dielectric constants, respectively. $\tau_{\tan\delta}$ is the relaxation time and $\omega$ is the angular frequency of the applied field. From Debye equation, the loss factor exhibits a maxima when $\omega\tau_{\tan\delta} = 1$ which provides the frequency, $f_m$ (=$1/2\pi\tau_{\tan\delta}$), at which the maximum loss occurs. The temperature dependence of loss peak satisfies Arrhenius law, i.e., $f_m = f_0 \exp(-E_{\tan\delta}/k_B T)$, where $k_B$ is Boltzmann constant and $E_{\tan\delta}$ is the activation energy for loss to occur. It is observed from Fig. 4(b) that the dielectric loss increases with increase in the concentration of $Mg^{2+}$ ions. This can be explained on the basis that the conduction mechanism is same as that of dielectric polarization and the conduction loss increases due to increased number of $Fe^{2+}$–$Fe^{3+}$ ion pairs causing an increased hopping of electrons between these ions [26]. From Fig. 4(b), it is also observed that all the samples show dispersion in tan $\delta$ at lower frequencies with a peak appearing at nearly same frequency at a given temperature implying the composition independence of the loss peak.

### 3.4. Conduction mechanism

The total conductivity can be represented by the formula

$$\sigma(\omega, T) = \sigma_{dc}(T) + \sigma_{ac}(\omega, T) = \sigma_{dc}(T) + B(T)\omega^{s(T)} \quad (6)$$

where $\sigma_{dc}$ is the dc conductivity, $\sigma_{ac}$ is the ac conductivity, $B(T)$ is the temperature dependent quantity and $s(T)$ is the universal power law exponent lying in the range from 0 to 1. Fig. 5(a) shows the frequency dependence of total conductivity for $x = 0.1$ sample at different temperatures. All other samples also show qualitatively similar variation of $\sigma$ with frequency. This plot shows that the conductivity remains almost constant in the low frequency region but exhibits dispersion for higher frequencies, which is in accordance with Eq. (6). This dispersion in conductivity shifts towards higher frequency with increase in temperature. As mentioned earlier, the mechanism of electrical conduction is same as that of dielectric polarization. In the low frequency region, grain boundaries with high resistance are effective, giving a constant plateau region ($\sigma_{dc}$). At higher frequencies, the increase in conductivity is due to grain effect and increased hopping of charge carriers between $Fe^{2+}$–$Fe^{3+}$ ions at the adjacent octahedral sites [29]. The increase in conductivity with temperature is due to thermally activated hopping of charge carriers [6]. The increase in conductivity with increase in the concentration of $Mg^{2+}$ ions is due to the increase in the magnitude

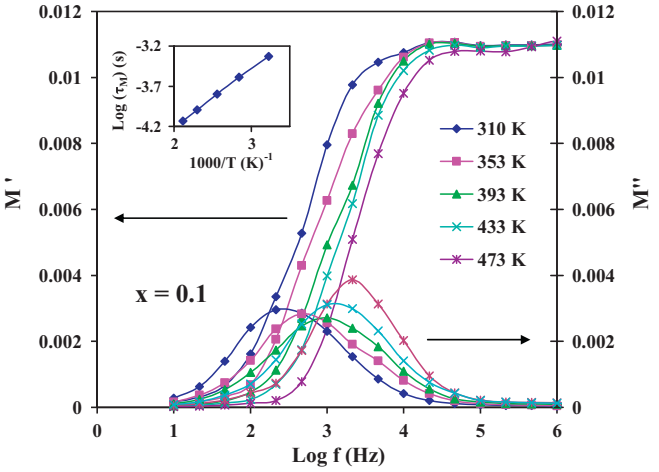


**Fig. 6.** Frequency dependence of the real and imaginary part of electric modulus for $x = 0.1$ at different temperatures. Inset: Arrhenius plot for the relaxation time $\tau_M$ for $x = 0.1$.

of electronic exchange which is dependent on the concentration of $Fe^{3+}/Fe^{2+}$ ion pairs present on B-site (Fig. 5(b)).

The dc conductivity, $\sigma_{dc}$ was calculated from the total conductivity data and using the sample dimensions. Inset in Fig. 5(a) shows the Arrhenius plots for $\sigma_{dc}$ for different samples and it is observed

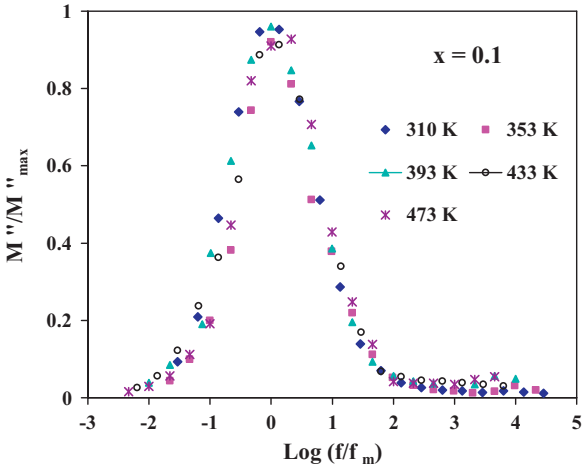


**Fig. 7.** Normalized plots of dielectric modulus versus normalized frequency for $x = 0.1$ at various temperatures.

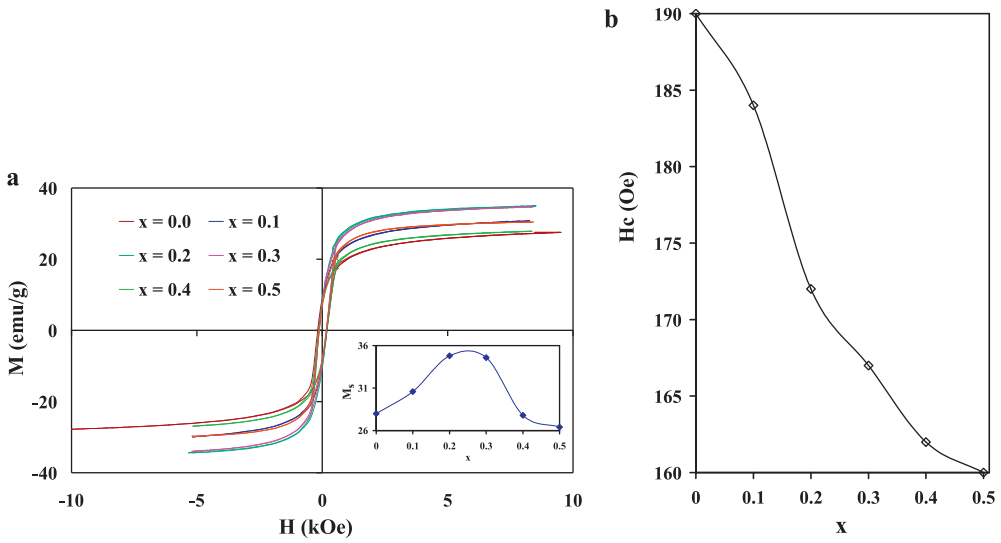


**Fig. 8.** (a) Hysteresis curve for $Ni_{0.5}Li_{1-2x}Mg_xFe_2O_4$ ferrites. Inset: Composition dependence of saturation magnetization ($M_s$). (b) Composition dependence of coercivity ($H_c$).

that $\sigma_{dc}$ increases with increase in temperature. An apparent one slope over the entire set of measurement is an evidence of a single conduction mechanism, i.e., in the present study, hopping of charge carriers is responsible for electronic conduction. The activation energy required for hopping process is calculated from the Arrhenius relation:

$$\sigma_{dc} = \sigma_0 \ \exp\left(\frac{-E_{dc}}{k_B T}\right) \tag{7}$$

The activation energy, $E_{dc}$ was calculated from the least square straight line fitting of plots shown as the inset of Fig. 5(a) and the values of $E_{dc}$ are included in Table 1. It is observed from the inset of Fig. 5(a) and Table 1 that the $\sigma_{dc}$ increases with increase in $x$. Since the dielectric constant is roughly proportional to the inverse of the square root of resistivity [19], therefore, such variations are expected. Both the dielectric constant and electrical conductivity, being transport properties, show similar variations with composition and the same mechanism is responsible for this phenomenon. The values of $\sigma_{ac}$ (at 310 K, $10^5$ Hz) for all the samples are given in Table 1. On the comparison of the values of $\sigma_{dc}$ and $\sigma_{ac}$ (Table 1), it is observed that the magnitude of ac conductivity is about 2–3 times higher than that of dc conductivity at all the compositions.

### 3.5. Electrical modulus studies

The electrical modulus formalism is widely used to study electrical relaxation in electronically and ionically conducting materials as it has advantage of suppressing electrode polarization effects. Electric modulus ($M^*$) is defined as the reciprocal of dielectric permittivity and is given by following relation:

$$M^*(\omega) = \frac{1}{\varepsilon^*(\omega)} = \left\{\varepsilon'(\omega) - i\varepsilon''(\omega)\right\} \left|\varepsilon^*(\omega)\right|^2 = M'(\omega) + iM''(\omega)$$
$$M_\infty(\omega) = \left[1 - \int_{-\infty}^{\infty} e^{-i\omega t} \left\{\frac{d\Phi}{dt}\right\} \ dt\right] \tag{8}$$

where $M'(\omega)$ and $M''(\omega)$ are the real and imaginary parts of the electrical modulus, respectively, $M_\infty$ (=$1/\varepsilon_\infty$) is the inverse of the high-frequency dielectric permittivity. $\Phi(t)$ is the relaxation function which evolves the electric field within the dielectric and is related to relaxation time by decay function proposed by Kohlrausch–Williams–Watts (KWW) [30,31] and is given by

$$\phi(t) = e^{[-(t/\tau_M)^\beta]} \tag{9}$$

where $\tau_M$ is the most probable relaxation time and $\beta$ is the stretched exponent parameter. The value of $\beta$ determines whether Debye or non-Debye type of relaxation is present in a given material [32,33] and is related to full width at half maximum of a suitably normalized frequency dependent $M''(\omega)$ curves. The imaginary part of electrical modulus $M''(\omega)$ is related to the energy dissipation taking place during irreversible conduction process [5].

The frequency dependence of real ($M'$) and imaginary ($M''$) parts of the electrical modulus at various temperatures for $x = 0.1$ sample is shown in Fig. 6. Qualitatively similar frequency dependence for $M'$ and $M''$ was observed in other samples. $M'(\omega)$ exhibits small values in the low frequency region which reveals polaron hopping and for moderate frequencies, $M'(\omega)$ shows a dispersion tending to $M'_\infty$ in the high frequency region. $M''(\omega)$ shows an asymmetric maximum at frequency $f_{M''}$ centered at the dispersion region of $M'(\omega)$, revealing maximum conduction loss. The characteristic frequency at which $M''(\omega)$ is maximum ($M''_{max}$) corresponds to relaxation frequency and is used for the evaluation of relaxation time, $\tau_{M''}$ (=$1/2\pi f_{M''}$). The maximum in the $M''(\omega)$ curves shifts towards higher frequencies as the temperature increases implying an increase in relaxation rate because of thermal activation of charge carriers. The reciprocal temperature dependence of $\tau_{M''}$ also satisfies the Arrhenius relation $\tau_{M''} = \tau_0 \exp(E_{M''}/k_B T)$ and is shown in the inset of Fig. 6. The activation energy for the conductivity relaxation time, $E_{M''}$ has been calculated from the least square fitting of data and its values are presented in Table 1. It is observed from Table 1 that the values of activation energies for conductivity relaxation ($E_{M''}$) and for dc conduction ($E_{dc}$) are nearly same which suggests that the mechanism of electrical conduction and dielectric polarization is same in these ferrites. Similar results have also been reported for Ni–Zn ferrites [5].

The value of $\beta$ is equal to 1 for an ideal dielectric where dipole–dipole interaction is negligible and for the system where this interaction is significant, $\beta < 1$. In the present ferrites, the value of $\beta < 1$ (Table 1) which suggests that the non-Debye type of relaxation prevails in these ferrites [5,32]. Fig. 7 shows the normalized plots of the imaginary part of the electric modulus ($M''$), where the frequency axis is scaled by the peak frequency and $M''$ axis is scaled by $M''_{max}$. A prefect overlapping of all the curves on a single master curve is observed for all the temperatures. This again confirms that the single relaxation process occurs at different frequencies and the dynamic processes are temperature independent.

### 3.6. Magnetic properties

The hysteresis loops of all the annealed Ni–Li–Mg ferrites are shown in Fig. 8(a). The values of saturation magnetization and coercivity were calculated using these plots and are included in Table 1. The variation of saturation magnetization ($M_s$) with $x$ is shown as an inset of Fig. 8(a). It is observed that the saturation magnetization ($M_s$) increases up to $x = 0.2$ and for $x \geq 0.3$, it decreases. The observed magnetization is a result of the simultaneous influence of several extrinsic and intrinsic factors such as density, anisotropy, grain size, cation distribution and the A–B exchange interaction [33,34]. The saturation magnetization is, therefore, explained by considering the metal ion distribution and antiparallel spin alignment of the two sublattice sites. According to Neel's model, of the three types of AA, AB and BB interactions, intersublattice A–B superexchange interaction is the strongest. The net magnetization is given by the vector sum of the magnetization of the two sublattices A and B, i.e., $M = M_B - M_A$, where $M_A$ and $M_B$ are the magnetizations of the sublattices A and B, respectively. The initial increase in $M_s$ may be due to the fact that some of the $Mg^{2+}$ ions, which are incorporated in place of $Li^+$ ions, occupy tetrahedral site (A) in the spinel lattice with a corresponding migration of $Fe^{3+}$ ions from A-site to B-site. This increases the magnetization of the B sublattice while that of A sublattice decreases as $Fe^{3+}$ ions have a magnetic moment = 5 $\mu_B$ and $Li^+$ and $Mg^{2+}$ ions are non-magnetic. With further incorporation of $Mg^{2+}$ ions ($x \geq 0.3$), the decrease in $M_s$ can be attributed to the increased migration of $Fe^{3+}$ ions from the A- to B-site in order to accommodate the $Mg^{2+}$ ions at the A-site. This migration results in an increase in $Fe^{3+}$ ion concentration at B-site which gives rise to antiparallel spin coupling and spin canting. This results in the weakening of the A–B exchange interaction, leading to the reduction of the magnetization. Fig. 8(b) shows the variation of coercive field ($H_c$) with $x$ and it is observed that $H_c$ decreases with the increase in the concentration of $Mg^{2+}$ ions. This may be attributed to loss of anisotropy due to the migration of $Mg^{2+}$ ions to tetrahedral site [20,34,35].

## 4. Conclusions

Nanoparticles of $Ni_{0.5}Li_{1-2x}Mg_xFe_2O_4$ ($0.0 \leq x \leq 0.5$) ferrites have been prepared successfully by sol–gel auto combustion technique. The XRD patterns reveal the spinel structure of the annealed ferrites. Dielectric constant ($\varepsilon'$) decreases with the increase in the frequency of external electric field and increases with temperature. The variation of dielectric loss with frequency shows a peak. Conductivity is found to increase very slowly at low frequencies and abruptly at high frequencies. The dc and ac conductivities of these ferrites increase with the increase in temperature and concentration of $Mg^{2+}$ ions due to the increased hopping of electrons between $Fe^{2+}$ and $Fe^{3+}$ ions. Nearly similar values of activation energy for dc conduction and for conductivity relaxation suggest that the mechanism of electrical conduction and dielectric relaxation are identical. The value of the stretched exponent parameter $\beta$ is less than 1 which reveals the presence of non-Debye type of relaxation in the present ferrites. Saturation magnetization first increases with the increase in the concentration of $Mg^{2+}$ ions due to increased magnetization of B-site and then decreases because of the antiparallel spin coupling. Coercivity values are found to decrease with the incorporation of $Mg^{2+}$ ions.

## Acknowledgements

Authors are thankful to CSIR and DST (FIST scheme), New Delhi for providing financial support.

## References

[1] M.P. Horvath, J. Magn. Magn. Mater. 215 (2000) 171.
[2] I. Soibam, S. Phanjoubam, H.B. Sharma, H.N.K. Sharma, R. Laishram, C. Prakash, Solid State Commun. 148 (2008) 399.
[3] S.A. Mazen, S.F. Mansour, E. Dhahri, H.M. Zaki, T.A. Elmosalami, J. Alloys Compd. 470 (2009) 294.
[4] T. Nakamura, M. Naoe, Y. Yamada, J. Magn. Magn. Mater. 305 (2006) 120.
[5] N. Sivakumar, A. Narayanasamy, N. Ponpandian, G. Govindaraj, J. Appl. Phys. 101 (2007) 084116.
[6] R.G. Kharabe, R.S. Devan, B.K. Chougale, J. Alloys Compd. 463 (2008) 67.
[7] I. Soibam, S. Phanjoubam, C. Prakash, J. Magn. Magn. Mater. 321 (2009) 2779.
[8] M.F. Al-Hilli, S. Li, K.S. Kassim, Mater. Sci. Eng. B 158 (2009) 1.
[9] S.S. Bellad, B.K. Chougule, Mater. Chem. Phys. 66 (2000) 58.
[10] S. Verma, J. Karande, A. Patidar, P.A. Joy, Mater. Lett. 59 (2005) 2630.
[11] A. Ataie, I.R. Harris, C.B. Ponton, J. Mater. Sci. 30 (1995) 1429.
[12] M.M. Hessien, M.M. Rashad, K. El-Barawy, J. Magn. Magn. Mater. 320 (2008) 336.
[13] C. Surig, K.A. Hempel, D. Bonnenborg, IEEE Trans. Magn. 30 (1994) 4092.
[14] M.C. Dimri, A. Verma, S.C. Kashyap, D.C. Dube, O.P. Thakur, C. Prakash, Mater. Sci. Eng. B 133 (2006) 42.
[15] L.J. Berchmans, R.K. Selvan, C.O. Augustin, Mater. Lett. 58 (2004) 1928.
[16] P.P. Hankare, R.P. Patil, U.B. Sankpal, S.D. Jadhav, K.M. Garadkar, S.N. Achary, J. Alloys Compd. 509 (2011) 276.
[17] P.P. Hankare, R.P. Patil, U.B. Sankpal, S.D. Jadhav, P.D. Lokhande, K.M. Jadhav, R. Sasikala, J. Solid State Chem. 182 (2009) 3217.
[18] P.P. Hankare, R.P. Patil, U.B. Sankpal, S.D. Jadhav, I.S. Mulla, K.M. Jadhav, B.K. Chougule, J. Magn. Magn. Mater. 321 (2009) 3270.
[19] R.G. Kharabe, R.S. Devan, C.M. Kanamadi, B.K. Chougule, Smart Mater. Struct. 15 (2006) N36.
[20] J. Jing, L. Liangchao, X. Feng, J. Rare Earths 25 (2007) 79.
[21] B.D. Cullity, Elements of X-ray Diffraction, Addison-Wesley, Reading, 1978.
[22] M. Maisnam, S. Phanjoubam, H.N.K. Sarma, C. Prakash, L.R. Devi, O.P. Thakur, Physica B 370 (2005) 1.
[23] C.G. Koops, Phys. Rev. 83 (1951) 121.
[24] P.V. Reddy, V.D. Reddy, J. Magn. Magn. Mater. 136 (1994) 279.
[25] C.S. Narasimhan, C.S. Swamy, Phys. Status Solidi (a) 59 (1980) 817.
[26] P.V. Reddy, T.S. Rao, J. Less Common Met. 86 (1982) 255.
[27] A.M. Shaikh, S.S. Bellad, B.K. Chougule, J. Magn. Magn. Mater. 195 (1999) 384.
[28] D. Ravinder, P.V.B. Reddy, Mater. Lett. 57 (2003) 4344.
[29] H. Bottger, V.V. Bryksin, Hopping Conduction in Solids, Akademie-Verlag, Berlin, 1985.
[30] R. Kohlrausch, Pogg. Ann. Phys. Chem. 91 (1854) 179.
[31] G. Williams, D.C. Watts, Trans. Faraday Soc. 66 (1970) 80.
[32] N. Ponpandian, A. Narayanasamy, J. Appl. Phys. 92 (2002) 2770.
[33] M.M. Hessien, J. Magn. Magn. Mater. 320 (2008) 2800.
[34] R.G. Kharabe, S.A. Jadhav, A.M. Shaikh, D.R. Patil, B.K. Chougule, Mater. Chem. Phys. 72 (2001) 77.
[35] J. Jiang, Y. Yang, L. Li, J. Alloys Compd. 464 (2008) 370.